JOURNAL OF GEOPHYSICAL RESEARCH, VOL. 103, NO. D18, PAGES 23,231-23,242, SEPTEMBER 27, 1998

Airborne retrieval of cirrus cloud optical and microphysical properties using Airborne Remote Earth Sensing System 5.1-5.3 and 3.7-μm channel data

S. C. Ou,[1] K. N. Liou, [1] P. Yang, [1] P. Rolland, [1] T. R. Caudill, [2]
J. Lisowski, [3] B. Morrison, [4]

Abstract. We present an airborne retrieval algorithm to infer cirrus cloud temperature, optical depth, and mean effective sizes using the Airborne Remote Earth Sensing System (ARES) hyperspectral spectrometer data for the 5.1-5.3 and 3.7 μm channels. The algorithm development and the selection of the channels are based on the principle and parameterization of radiative transfer involving cirrus clouds and the associated atmospheric and surface properties. It has been applied to a selected case of the ARES data collected over the western Boston area on September 16, 1995. Validation of the retrieved parameters was carried out using the collocated and coincident ground-based 8.6-mm radar data and ice crystal size distribution measurements obtained from the 2D-P probe on board the high-altitude reconnaissance platform (HARP). We show that the retrieved cirrus cloud temperature, mean effective ice crystal size, and optical depth match closely with those derived from the observations.

1. Introduction

Established cirrus cloud retrieval methods based on imaging radiometric data generally use the visible, window (e.g., 3.7, 10.9, and 12.0 μm), and water vapor absorption (6.3 μm) channel radiances that are available from either operational satellites or research aircraft [*Liou et al.*, 1990; *Minnis et al.*, 1990, 1993; *Baum et al.*, 1994; *Ou et al.*, 1993, 1995]. Remote sensing of the cirrus cloud parameters using radiances from other spectral channels has also been recently explored. *Wielicki et al.* [1993] investigated the possibility of using the 0.83 and 1.65 μm radiances from Landsat to determine ice crystal particle sizes. *Gao and Kaufman* [1995] reported a new technique for detecting thin cirrus clouds using the 1.38 and 1.88 μm water vapor absorption channels radiances from the airborne visible infrared imaging spectrometer (AVIRIS), based on the fact that the low-level water vapor absorption provides a dark background for the high-altitude cirrus reflection to be detectable. The 1.6 and 2.2 μm channel radiances from the moderate resolution imaging spectroradiometer (MODIS) and the MODIS airborne simulator (MAS) are also potentially useful channels for future developments of cirrus cloud retrieval algorithms [*King et al.*, 1992, 1995; *Tsay et al.*, 1996], because both wavelengths are sensitive to variations in ice crystal size distributions. Moreover, the selection of appropriate channels for reliable cirrus cloud detection and retrieval will be a major consideration in the development of the National Polar-Orbiting Operational Environmental Satellite System (NPOESS) project.

Recently, the Airborne Remote Earth Sensing System (ARES) hyperspectral spectrometer data collected at various observational sites have been published. These data contain radiances for certain spectral intervals that have not been explored previously for the development of cloud retrieval algorithms. To investigate the applicability of remote sensing of cirrus cloud parameters using ARES data, an airborne retrieval algorithm to infer cirrus cloud temperature, optical depth, and ice crystal mean effective size has been developed. The retrieval method utilizes for the first time the 5.1-5.3 μm water vapor band to determine cirrus cloud temperatures and IR emissivities, from which the associated optical depths can be determined from radiative transfer parameterizations. In the scheme, the ice crystal mean effective size is derived by matching the sum of the computed 3.7 μm solar reflected and IR emitted radiances with the ARES 3.755 μm (channel 42) radiances. The selection of these retrieval channels is based on the examination of the computed weighting functions of a typical midlatitude summer atmosphere along with the inspection of ARES channel radiance images. We

[1]Department of Atmospheric Sciences, University of California, Los Angeles, Los Angeles.
[2]Air Force Research Laboratory/VSBE Hanscom Air Force Base, Massachusetts.
[3]SciTec, Inc. Princeton, New Jersey.
[4]Aeromet, Inc. Tulsa, Oklahoma.

Paper number 98JD02069.
0148-0227/98/98JD-02069$09.00

have applied the retrieval algorithm to the ARES data collected during a mission flight, which was carried out on board the WB-57F aircraft on September 16, 1995, over the western Boston area. The retrieved cloud parameters are compared with the in situ 2D-probe measurements obtained from the Aeromet's high-altitude reconnaissance platform (HARP), as well as the cloud heights derived from the ground-based 8.6-mm radar returns.

Cloudy radiances have been measured by the IR imaging spectrometer/radiometer on board the ARES Program's WB-57F high-altitude research aircraft operated by the NASA Johnson Space Center. The WB-57F is capable of reaching altitudes in excess of 60,000 feet (18,300 m), and carries a crew of two, permitting instrument operation by a dedicated flight crew. The sensor was mounted on the lower fuselage surface, with downward viewing while in level flight. The ARES sensor for the present study has been operated as a 75-channel imaging spectrometer. It is operated in a push broom mode with 45-pixel array pointing in the nadir direction taking data at the standard rates of 10, 20, 40, or 80 scans/s. The optical elements of ARES provide a pixel IFOV (instantaneous field of view) of slightly more than 1 mrad, which corresponds to about 15 m ground resolution for a flight altitude of 15 km. The spacing of the ARES spectral wavelengths appears to depend on the optical arrangement with the channel bandwidths that vary between 0.02 and 0.07 μm. Further details of ARES can be obtained from the internet Web site: http://cahill.plh.af.mil:8600/PDAC.html.

For validation of the retrieved cloud height, we have obtained the cloud boundary height data from the collocated and coincident ground-based 8.6-mm TPQ-11 radar measurements. For comparison of the retrieved cloud optical depth and mean effective sizes with in situ measurements, we have also acquired the meteorological and ice microphysical data collected from HARP, which is a Learjet 36A, flying in conjunction with the ground-based radar and the ARES measurements. HARP carried instruments for taking both in situ and remote atmospheric measurements. The in situ instruments include forward scattering spectrometer probe (FSSP) 1D-C and 2D-C probes for particle size distribution measurements. Ambient temperatures were measured by the Rosemount total temperature sensor with an uncertainty of ± 1 K.

This paper is organized as follows. In section 2, we describe the development of the remote sensing algorithm for the retrieval of cirrus cloud temperature (height), optical depth, and ice crystal size principally using the ARES 5.1-5.3 and 3.7 μm channels. In section 3, results of the application of this retrieval scheme to the ARES data collected during September 16, 1995, are presented along with the validation efforts using the ground-based radar and airborne in situ measurements. Finally, a summary is given in section 4.

2. Principle of Retrieving Cirrus Parameters Using ARES Thermal IR Channels

The present retrieval method for inferring cirrus temperature and emissivity is based on the numerical solution of the following set of algebraic equations [*Liou et al.*, 1990; *Ou et al.*, 1993, 1995] :

$$R_i = (1 - \varepsilon_i) R_{ai} + \varepsilon_i B_i(T_c) \tag{1}$$

$$\varepsilon_i = 1 - \exp(-k_i \tau) \tag{2}$$

where R_i are the upwelling radiances at the top of the cirrus cloudy atmosphere for the ith selected ARES channel; R_{ai} are the corresponding radiances reaching the cloud base for the ith channel; ε_i are the cloud IR emissivities, T_c is the mean cirrus temperature; $B_i(T_c)$ are the Planck intensities at T_c, τ is the visible optical depth, and k_i is the effective extinction coefficient that has been determined from the calculated single-scattering properties based on a number of measured ice crystal size distributions. The behavior of the cloud emissivity in terms of its dependence on wavelength and cloud parameters has been examined previously [*Liou et al.*, 1990].

By straightforward algebraic analyses, equations (1) and (2) for a pair of channels ($i = 1$ and 2) can be combined into a single equation in the form

$$[R_2 - B_2(T_c)]/[R_{a2} - B_2(T_c)] = \{[R_1 - B_1(T_c)]/[R_{a1} - B_1(T_c)]\}^{k_2/k_1}. \tag{3}$$

If R_{a1} and R_{a2} are known, $B_2(T_c)$ and $B_1(T_c)$ are approximately linearly correlated, and $k_2/k_1 \sim 1.0$, then (3) becomes a linear equation, whose numerical solution can be obtained in a relatively straightforward manner.

The effective extinction coefficients for the retrieval channels have been computed using the adding/doubling program in conjunction with the development of this remote sensing algorithm. Eleven ice crystal size distributions from aircraft in situ measurements have been chosen [*Fu and Liou*, 1993]. Their mean effective ice crystal sizes range between 23.9 and 123.6 μm. The single-scattering properties including phase functions, single-scattering albedos, and extinction coefficients have been computed for each size distribution and for each of the selected ARES channels using the unified theory for light scattering by ice crystals [*Yang and Liou*, 1996a, b]. To optimize the computational effort, the forward scattering peak of each phase function was truncated following the procedure developed by *Takano and Liou* [1989]. Radiances for each channel and for a range of optical depths and ice crystal sizes were computed using the aforementioned adding/doubling program. The cirrus cloud emissivity, which is defined as the ratio of the upwelling radiance to the cloud Planck function, was obtained as functions of the optical depth, mean effec-

tive size, and channel wavelengths. Finally, the effective extinction coefficients for each channel and for each size distribution was obtained as the slope of the linear curve fitting of $-\ln(1-\varepsilon_i)$ versus τ. Figure 1 shows the effective extinction coefficient (k value) as a function of the mean effective size for eight wavelengths. For all wavelengths, the k values increase with the mean effective size. This functional dependence of the k values has been incorporated into the retrieval program. More importantly, the diagram indicates that the values of the three pairs of k ratios, k(5.189 μm)/k(5.116 μm), k(5.261 μm)/k(5.116 μm), and k(5.332 μm)/k(5.116 μm), depend weakly on the mean effective size and are all close to 1.0 for the range of the mean effective size considered here. Thus, they are fixed at 1.0 in the numerical solution of (3).

In order to infer the cirrus emissivity, ε_i, and temperature, T_c, from multiple radiance measurements in cloudy conditions, the upwelling radiances at the cloud base, R_{ai}, must be known. In principle, it can be generated from forward radiation transfer calculations if the surface temperature, atmospheric temperature and humidity profiles, and cloud base height are given. However, a more direct and reliable method to determine R_{ai} would be to find clear column radiances from the available data.

Assuming that the water vapor absorption/emission effects are negligible above cirrus clouds, we may approximate the cloud base upwelling radiance using the measured clear radiance at the ARES flight level. This approximation has been applied to the retrieval of cirrus cloud parameters using the AVHRR 3.7 and 10.9 μm window bands [*Ou et al.*, 1993] and to the airborne cirrus retrieval using the 6.5 and 10.5 μm radiometer data [*Liou et al.*, 1990]. Once R_{ai} is determined, (3) can be solved by a numerical iteration method to obtain T_c. Subsequently, ε_i is computed from (1). Since (1)-(3) apply to a pair of channel radiances, we form N-1 pairs of channel radiances, where $N(\geq 2)$ is the number of selected channels. The resulting N-1 sets of the retrieved temperature and emissivity are then averaged to obtain their respective mean values.

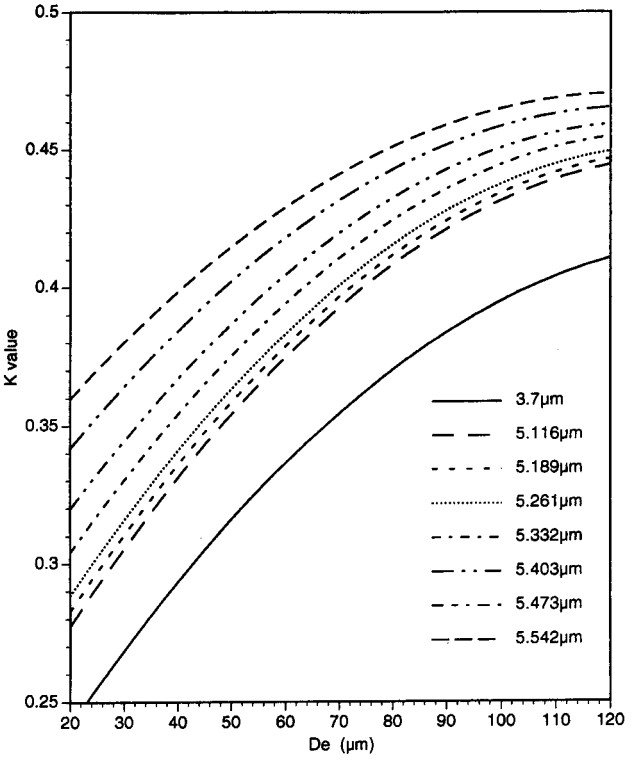

Figure 1. The k value as a function of D_e for the retrieval channels. Eleven size distributions have been used for single-scattering computations. The single-scattering properties are used in an adding/doubling code to obtain the cloud emissivity.

Upon retrieval of the IR emissivity and the cloud temperature using the thermal IR channels, we can obtain the mean effective size using the observed 3.7 μm channel radiances. We first assume a trial ice crystal size, from which the visible optical depth can be obtained from (2). The 3.7 μm thermal IR radiance can be calculated according to (1). The cloud base upwelling 3.7 μm IR radiance can be obtained by converting the 4.75 μm clear pixel radiance into its equivalent Planck function at 3.7 μm, since both channels are in the window spectral interval. The 3.7 μm solar reflectance is determined from look-up tables, which contain the computed value of the 3.7 μm solar reflectance as functions of the visible optical depth and the mean effective size. These tables are generated for the same six size distributions as described by *Rao et al.* [1995] and for appropriate solar-viewing geometries, using the adding/doubling method developed by *Takano and Liou* [1989]. Finally, the total 3.7 μm radiance is calculated as the sum of the thermal IR and solar radiances. The radiance values thus obtained are subsequently compared with the observed 3.7 μm radiances. The mean effective ice crystal size can then be obtained iteratively by adjusting the trial value based on the difference between the computed and observed radiances. Pixels having a retrieved mean effective size greater than 123.6 μm or less than 23.9 μm are discarded. Figure 2 gives a schematic flow diagram for the retrieval of cirrus cloud temperature, emissivity (optical depth) and mean ice crystal size.

3. Application of the Retrieval Scheme to the ARES Spectrometer Data

The preceding cirrus cloud retrieval scheme is applied to the ARES spectrometer data obtained during the WB-57F flight that was conducted on September 16, 1995. The flight has been divided into eight tracks. Data collected for tracks 1, 3, 5, and 8 were analyzed. These four tracks are straight, and spectrometer data were recorded in nadir-pointing push broom mode. The flight time for each track is 2055-2100 UTC (track 1), 2135-2140 UTC (track 3), 2212-2217 UTC (track 5), and 2308-2313 UTC (track 8). The cruise portion of each track was at an altitude of 15

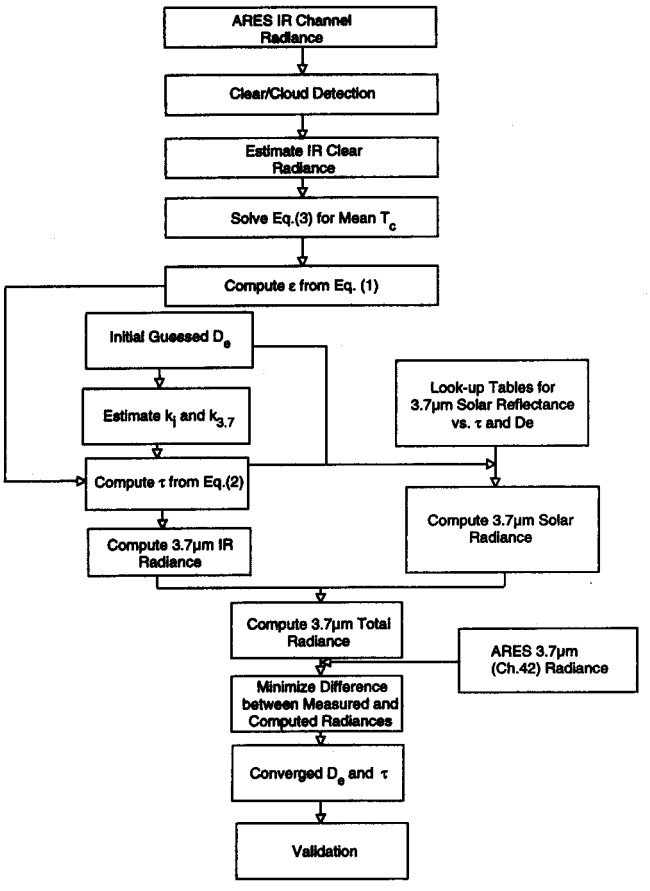

Figure 2. A schematic flowchart for the cirrus retrieval algorithm using ARES channel data.

km along the southeast-northwest direction, crossing over the Hanscom Air Force Base at Bedford, Massachusetts, where the ground-based 8.6-mm radar was located. During the period of tracks 1 and 3, HARP was also flying at the cirrus cloud level below the WB-57F. Between 2030 and 2040 UTC (case 1), and between 2147 and 2157 UTC (case 2), HARP flew in a racetrack pattern which was no more than 30 km from the Hanscom Air Force Base. Its flight tracks are approximately collocated and coincident with the route of ARES tracks 1 and 3, respectively. For both cases, the flight altitude was at about 8 km, close to the top of the cirrus cloud vertical domain.

3.1. ARES Channel Spectral Properties

Implementation of the preceding retrieval scheme requires understanding of the ARES channel spectral properties and the appropriate selection of useful ARES channel data. Figure 3 presents the upwelling radiances associated with solar reflection and thermal IR emission in the 2-6.4 μm region to assess the relative importance of the two radiation sources. For the solar reflection, we have used the updated solar irradiance data provided for our use by G. Anderson at the Air Force Geophysics Directorate [*Anderson*, 1995]. The results are shown for the cosine of two solar zenith angles and for a surface reflectance of 0.1. For the thermal IR emission, Planck function curves for three temperatures covering the range of relevant Earth's atmospheres are shown. It is clear that for $\lambda < 3$ μm, the solar reflection is the primary contributor to radiation, while for $\lambda > 4.5$ μm, the thermal IR emission is the predominant radiation source. For $3\ \mu\text{m} < \lambda < 4.5\ \mu$m, the relative importance of the solar reflection and thermal IR emission depends on the Sun's position, the surface albedo, and the atmospheric thermodynamic state. For the radiative transfer simulation and the remote sensing algorithm development, both components must be accounted for in this intermediate spectral range.

Based on the theory of atmospheric gaseous absorption, several absorption bands exist in the 2-6.4 μm spectral interval [*Goody and Yung*, 1989]. These include the 2.7 μm H_2O band produced by ν_1 and ν_2

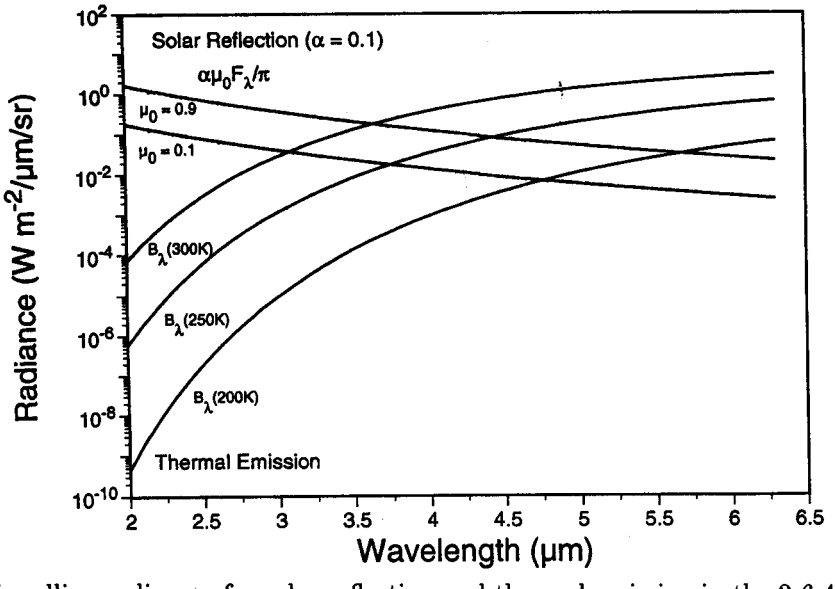

Figure 3. Upwelling radiances for solar reflection and thermal emission in the 2-6.4 μm region. F_λ denotes the solar irradiances, μ_o is the cosine of solar zenith angle, α is the surface albedo, and B_λ is the Planck function.

fundamentals, the 3.2 μm H_2O band associated with ν_2, the 4.3 μm CO_2 band due to the ν_3 fundamental and P and R branches, and the H_2O 6.3 μm vibrational (ν_2)-rotational band. There are three windows located at the 2.2, 3.7, and 4.7 μm regions. Figure 4 shows typical ARES 75-channel spectra obtained over clear and cirrus cloudy areas. Respective spectral intervals for the absorption bands are noted in the diagram. Large measurement noises exist for channels 1-25 (1.9-2.7 μm), where the solar reflection contributions are dominant and the cloud reflection is stronger than the surface reflection. For channels 26-75, the aforementioned four absorption bands and two window bands are clearly displayed as local minima and maxima, respectively, within both spectra. Over the 3.7 μm and 4.7 μm window bands and the 6.3 μm water vapor absorption band wing interval, there are significant differences between the clear and cloudy radiances. These differences can be used to detect the presence of cirrus clouds and to retrieve their optical and microphysical parameters.

3.2. Selection of Retrieval Channels

To select a number of appropriate channels for the cirrus cloud retrieval, we have examined all the ARES channel weighting function profiles and images. Typical weighting function profiles were generated using the vertical transmittance functions obtained from the MODTRAN calculations employing the climatological midlatitude summer temperature and humidity soundings. These weighting function profiles show features that correspond to the distribution of absorption bands. For the window channels (3.75 μm, and 4.7 μm), the weighting function peaks at or near the surface, so that the clear radiance is dominated by surface emission. The inhomogeneity of surface types and emissivity can cause clear radiance to spread, leading to errors in cloud retrieval results. For the 2.7 μm H_2O, 4.3 μm CO_2, and 6.3 μm H_2O band center channels, the weighting function peaks in the upper atmosphere. The radiance tends to be dominated by gaseous emission from the upper atmosphere, suppressing the cloud signals. For the 6.3 μm band wing channels, the weighting function peaks in the middle and lower troposphere. For the purpose of the detection and retrieval of cirrus clouds, it is advantageous to choose band wing channels with the weighting functions peaking in the lower troposphere, because the data spread in clear radiance would be narrow due to the blocking effect of the relatively homogeneous and moderate water vapor emission from the lower troposphere. In addition, the weighting function values from MODTRAN calculations are considerably smaller at or above cirrus altitude than at its peak level, indicating that the contribution of above-cloud water vapor absorption/emission to the upwelling radiance is likely to be small. Therefore, the emission from cirrus cloud subject to weak attenuation can be distinctly detected by satellite radiometers.

Moreover, we have used radiance images to facilitate the selection of channels by acquiring the ARES data collected on September 16, 1995 (data set 16-9-95-1A). Using a quick-look software ADAPT (ARES Data Analysis and Processing Toolkit developed by the SCITEC, Inc., at Princeton, New Jersey), we can display graphically the large volume of the ARES data set on a Silicon

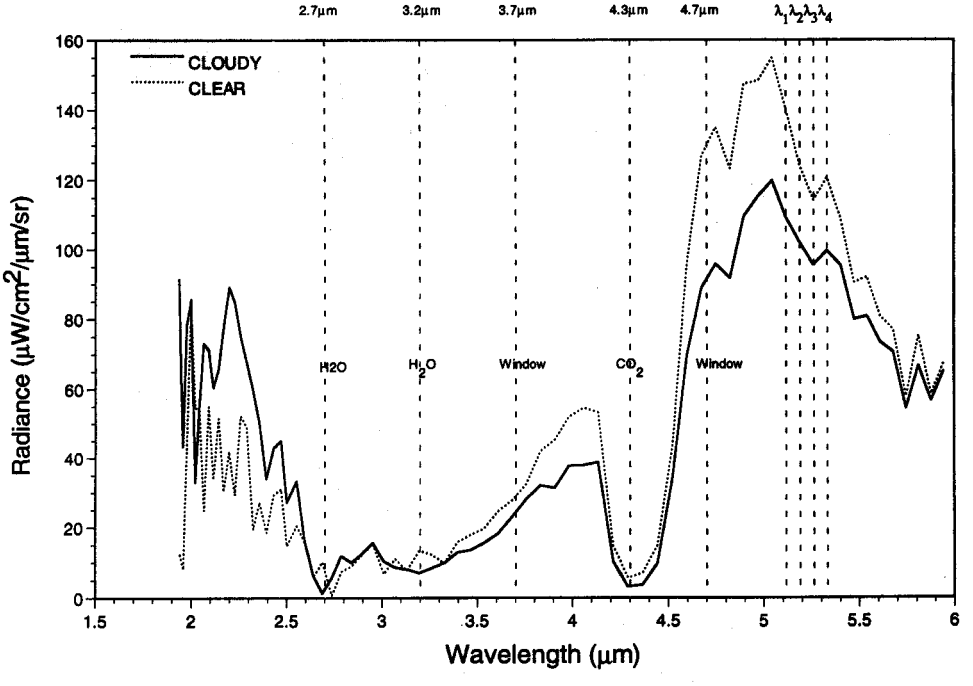

Figure 4. Typical ARES 75-channel spectra for clear and cloudy areas. The wavelengths λ_1, λ_2, λ_3, and λ_4 denote the four selected channels at 5.116, 5.189, 5.261 and 5.332 μm.

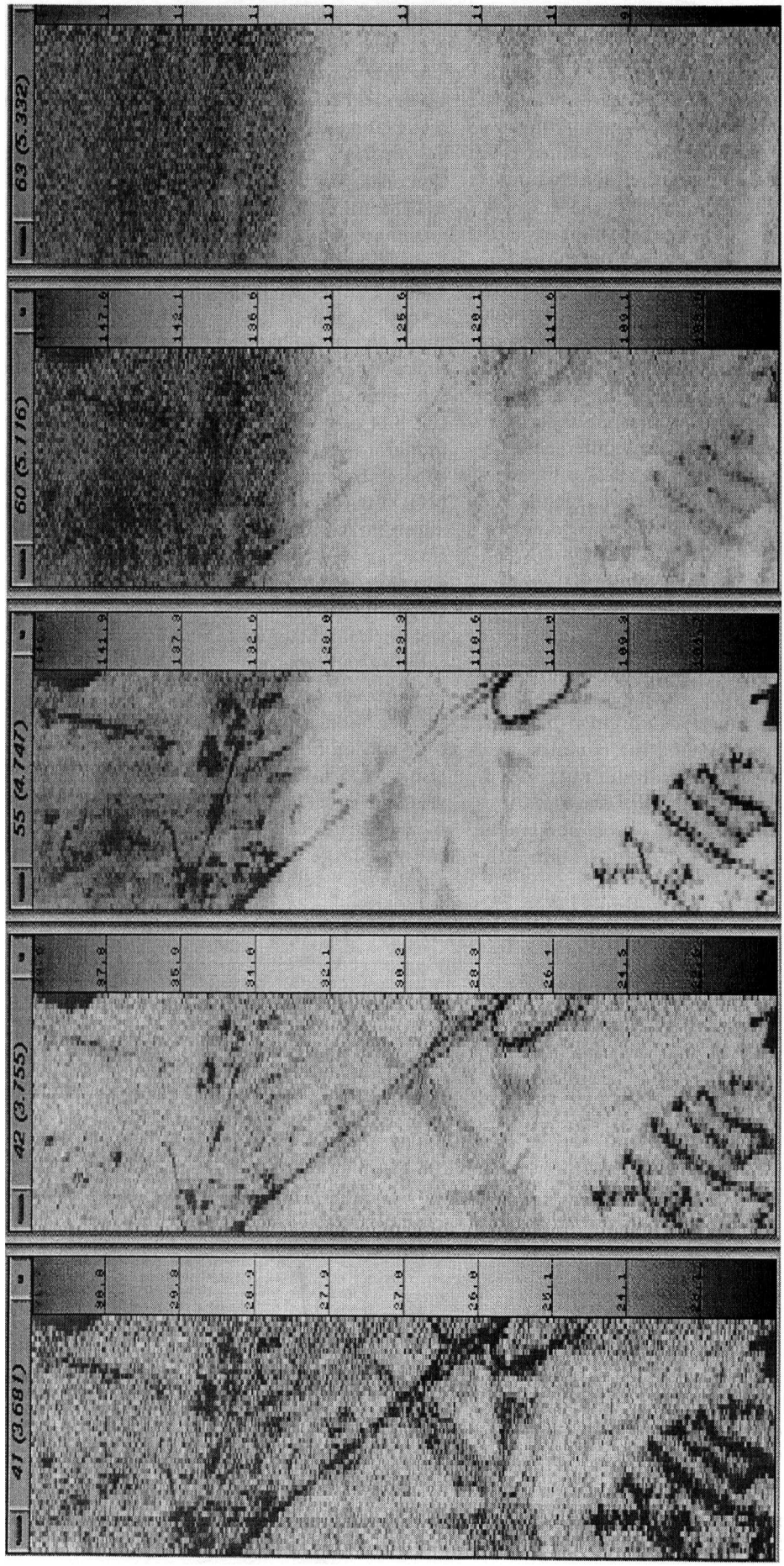

Figure 5. Radiance images for ARES wavelengths 3.681 μm (channel 41), 3.755 μm (channel 42), 4.747 μm (channel 55), 5.116 μm (channel 60), and 5.332 m (channel 63) over a section of the selected scene displaying a strong cloud/clear contrast within track 1 of the September 16 flight.

Graphic (SGI) system in imagery forms. We have manually examined the image of each flight track for each ARES channel, and have selected a scene which displays a distinct contrast between high- and low-radiance areas using the 4.747 μm channel imagery. Based on both ground-based 8.6 mm radar and airborne K_a band radar and 0.53 μm lidar observations on board HARP, only a single layer of cirrus cloud was present during the flight period. Thus, the high- and low-radiance areas correspond to clear and cloudy regions, respectively. Figure 5 shows the radiance images for 3.681 μm (channel 41), 3.755 μm (channel 42), 4.747 μm (channel 55), 5.116 μm (channel 60), and 5.332 μm (channel 63) wavelengths over a section of the selected scene. The first three channels are within the 3.75 μm and 4.7 μm window bands, while the last two channels are within the 6.3 μm water vapor band wing interval. For each image, the horizontal and vertical scales are $\sim$ 500 m and 2.5 km, respectively.

From these images, it is noted that the upper third of the domain is clear, while the rest of the domain is cloudy. Over the clear area, the images for the three window channels show significant variations of the emitted/reflected radiances due to the inhomogeneity of the surface temperature and emissivity. However, for the two band wing channels, radiances over the clear area appear to be relatively uniform, as compared to the clear radiances for the window channels. Although humidity sounding data were not available for the observation date, it is possible that the lower troposphere was humid on that date, and the resulting significant water vapor absorption/emission effect in the lower troposphere blocks the horizontally inhomogeneous surface emission. The narrow distribution of the clear radiances is a desirable feature for application of the remote sensing algorithm. A smaller spread in clear radiances would lead to smaller errors in prescribing the mean clear radiances, thus increasing the retrieval accuracy [*Rao et al.*, 1995].

Over the cloudy area, it is evident that the image for the 4.7 μm channel, as well as the images for the two band wing channels, contains distinct cloud signatures. For the two 3.7 μm window channels, there is no distinguishable cloud signature, because the compensating effects of the strong reflection and weak emission by cloud particles cause the resulting total cloud radiance to be about the same as the total clear radiance. Radiance images for channels at the absorption band center (not shown here) exhibit no cloud signature. Based on the preceding discussions on the properties of the computed weighting function profiles and the images shown in Figure 5, we select four wavelengths, 5.116 μm, 5.189 μm (channel 61), 5.261 μm (channel 62), and 5.332 μm, for the development of a cirrus cloud retrieval algorithm. The weighting function for these channels peaks in the lower troposphere, and images for these channels contain definitive cloud signatures and display narrow data spread of clear radiances.

3.3. Retrievals Using ARES Channel Data

In order to apply the aforementioned algorithm to the inference of the cloud temperature and emissivity, we must first determine clear or cloudy pixels within any selected scene. Thus, we have developed a clear/cloud detection scheme to identify clear and cloudy data points. It is based on the physical properties of the ARES equivalent brightness temperatures for selected channels for clear and cloudy pixels. In this scheme, clear pixels are separated from the cloudy pixels by applying the threshold tests to the equivalent brightness temperature data for each selected channel. If the equivalent brightness temperature for a pixel is greater than the prescribed threshold value for each selected channel, then it is categorized as clear. Otherwise, it is flagged as cloudy. The resulting number of cloudy pixels may be overestimated in this scheme. However, by doing so, we can ascertain that the detected clear pixels have the maximum probability to be truly clear, and that the maximum amount of cloudy pixels are available for the retrieval to be carried out.

Appropriate threshold values for the selected channels are determined from statistical analyses on the radiance data for the particular case of the mission flight on September 16, 1995. Figures 6a-6d show the histograms of the brightness temperatures for the four selected wavelengths within the domain of Figure 5. Each histogram displays a distinct bimodal shape due to the

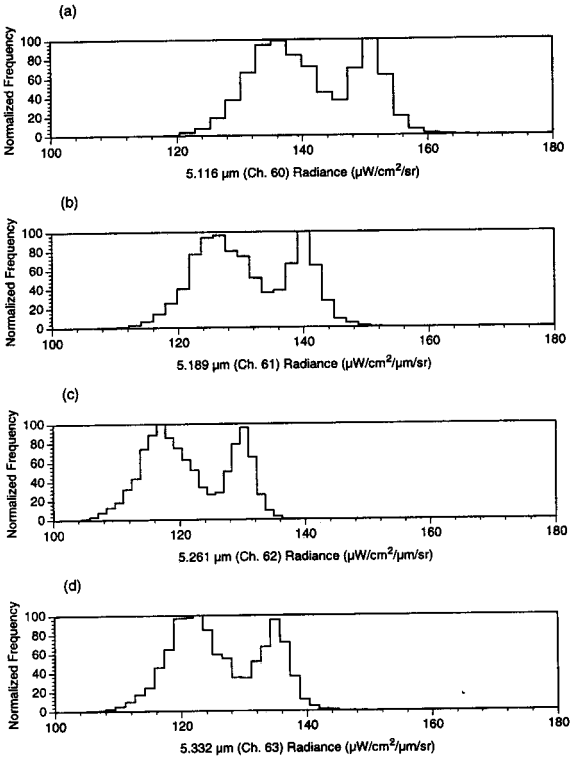

Figure 6. Histograms of the brightness temperatures for the ARES wavelengths 5.116 μm (channel 60), 5.189 μm (channel 61), 5.261 μm (channel 62) and 5.332 μm (channel 63) within the domain of Figure 5.

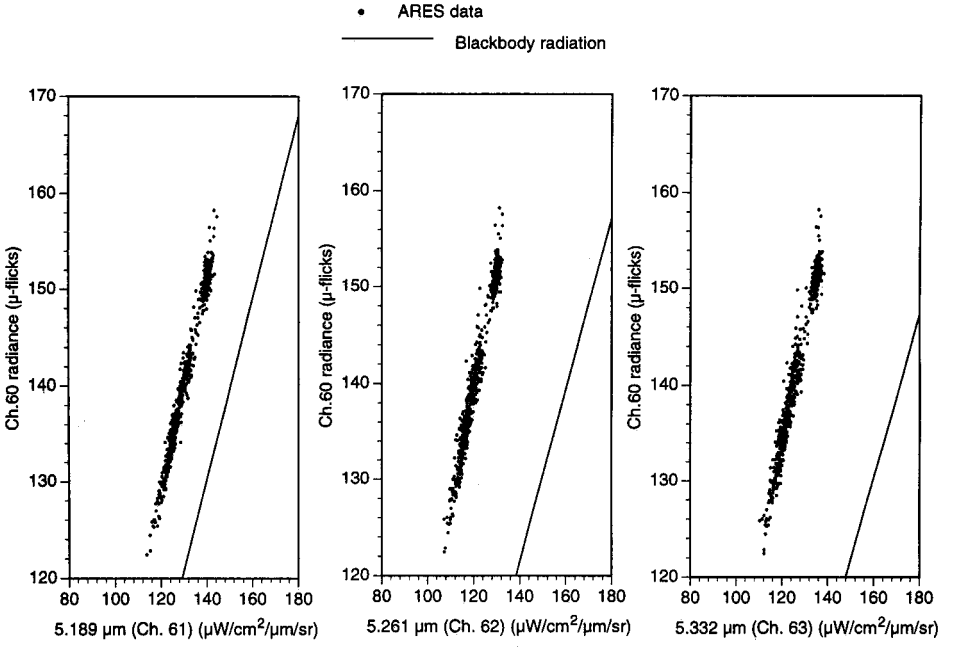

Figure 7. Examples of the scatter diagram for three pairs of ARES channels.

presence of contrasting clear and cloudy areas within the selected scene. As discussed previously, the high- and low-radiance modes represent the mean radiance for the clear and cloudy conditions, respectively. From these analyses, the threshold value for each channel is determined in a straightforward manner as the radiance that is associated with the minimum frequency between the two modes. Once the clear pixels are defined, the mean clear radiance for each channel is determined based on the average of radiance of all detected clear pixels within the selected scene (~10 km strip). It is possible that a small number of cloudy pixels may be misclassified as clear pixels, but inclusion of these pixels does not affect the determination of the mean clear radiance.

Next we investigate the characteristics of the measured ARES channel data. The ARES thermal IR channel data exhibit characteristics of linearity in the two-channel radiance correlation as implied in (3). Figure 7 shows the scatter diagram for the three pairs of ARES channels: 5.189 - 5.116 μm, 5.261 - 5.116 μm, and 5.332 - 5.116 μm. In each frame, the curve which is nearly linear denotes the correlation of Planck functions for the two channels, and the dots are radiance data points chosen from the scene of Figure 5 covering the area of the strong contrast between clear and cloudy regions. The manner in which radiance data points distribute in clusters indicates a statistically significant linear correlation between each pair of channel radiances. There are two clusters in each frame. The upper cluster corresponds to clear data points, while the lower elongated clusters are associated with cloudy radiances.

Figure 8 demonstrates the comparability of the measured and computed 3.7 μm channel radiances for the retrieval of mean effective sizes. In Figure 8a, the computed 3.7 μm solar radiances are plotted as functions of optical depth and six mean sizes. For $\tau > 2$, these radiances are nearly independent of the optical depth, but are strong functions of the ice crystal size distribution. In Figure 8b, the computed 3.7 μm thermal IR

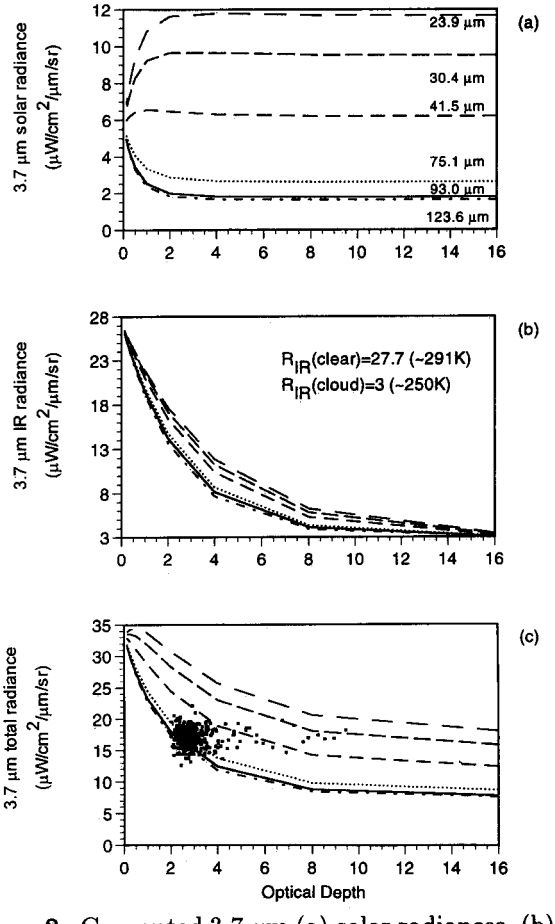

Figure 8. Computed 3.7 μm (a) solar radiances, (b) IR radiances, and (c) total radiances as functions of optical depth and ice crystal size.

radiances for different sizes are plotted against the optical depth. In this case, the cloud temperature is 250 K and the clear brightness temperature is 291 K. The 3.7 μm thermal IR radiances decrease with increasing optical depth and mean effective size. Finally, in Figure 8c, the computed 3.7 μm total radiances are plotted against the optical depth for the six ice crystal sizes. It is noted that for optical depth smaller than 10, and for ice crystal mean size less than 90 μm, these radiances are sensitive to both the optical depth and ice crystal size. We display the ARES measured data collected during track 3 of the September 16 flight in Figure 8c and show that they lie within the bulk range of the computed curves, indicating that it is feasible to use the ARES measured data to retrieve ice mean effective sizes. Data points that fall below the 123.6 μm curve were discarded during the retrieval.

Applying the retrieval scheme to the detected cloudy pixel radiance data of the selected ARES channels, we can determine the cirrus cloud temperatures and emissivities (optical depth) for the four flight tracks of September 16, 1995. By using an efficient numerical scheme, the total run time on a powerful state-of-the-art SGI is less than 10 min for each track. For the purpose of displaying data, we obtain the cross-track array-averaged channel equivalent brightness temperatures and the retrieved parameters for each scan within the flight track. Variation of the computed cross- track array-averaged 5.116 μm equivalent brightness temperatures, cloud temperatures, optical depths, and mean effective sizes for track 1 is shown in Figure 9 based on the application of the retrieval scheme to 10^4 scans of the 45-pixel array data. There are three periods which have been identified as clear (~16-20 km, 25-28 km, and 30-32 km). The retrieved cloud temperatures, optical depths, and mean effective ice crystal sizes vary between 230 and 260 K, between 0 and 2, and between 25 and 75 μm, respectively. Further examination of these retrieval results reveals that the cirrus cloud optical depths were generally less than 1.0, while the cirrus cloud temperatures were mostly higher than −30°C. The cirrus clouds were found to be composed of relatively small ice crystals. It is possible that these cirrus clouds were undergoing a formation stage, during which ice crystal sizes are usually small and clouds are optically thin. The reliability of the aforementioned retrieval results has been confirmed by the following validation efforts.

3.4. Validation of Retrieval Results

To validate the retrieved cirrus cloud height, we use the time series of cloud boundary (cloud top and base) altitudes derived from the 8.6-mm radar measurements, together with the upper tropospheric temperature measurement by the Rosemount total temperature sensor on board HARP. Figure 10a shows the atmospheric temperature at various levels between 5 and 11 km. These temperature values were obtained between 2029 and 2341 UTC. They vary between −5° and −55°C within the altitude range. This temperature profile is

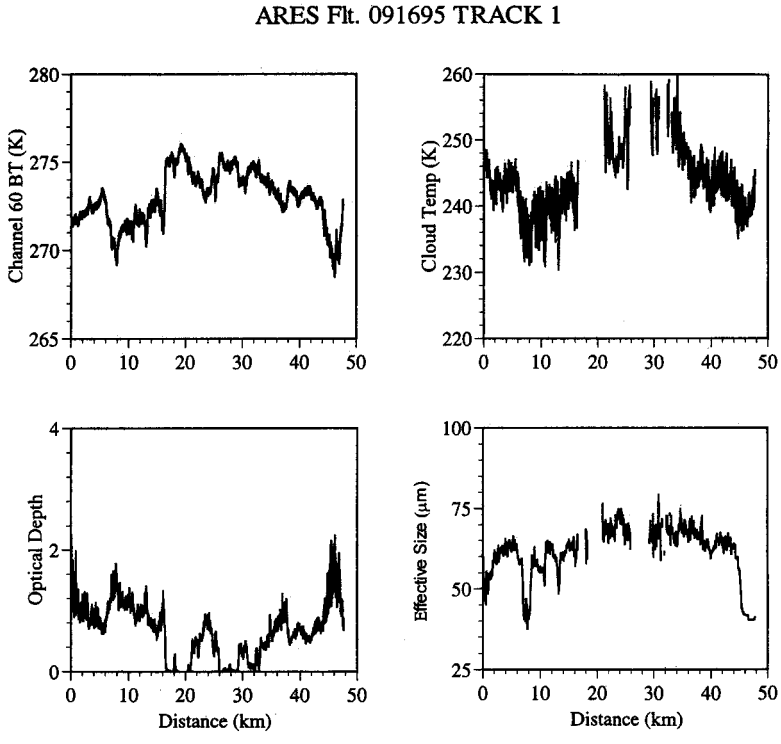

Figure 9. Cross-track array-averaged channel equivalent brightness temperatures, retrieved cloud temperature, cloud optical depth, and effective size as functions of flight distance for track 1, September 16, 1995.

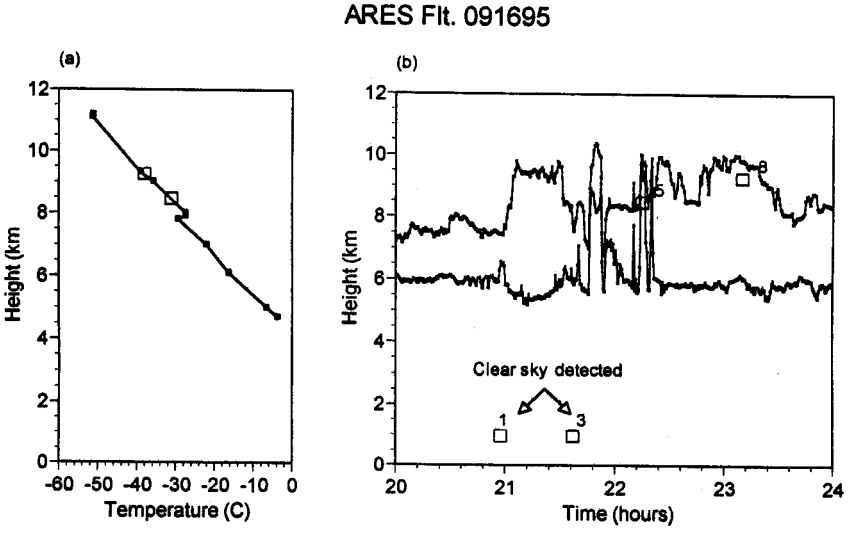

Figure 10. (a) Partial sounding of the middle and upper troposphere, obtained from the HARP flight above Hanscom Air Force Base (squares correspond to the retrieved cloud temperature). (b) Comparison of the cloud top heights obtained from radar/lidar measurements and the retrieved cloud temperatures. Retrieved temperatures are displayed for tracks 1, 3, 5, and 8 (in chronological order).

used in the validation effort because there was no surface sounding launched around the flight time of the WB-57F. We assume that the upper atmospheric thermal structure remained the same during the HARP flight period, so that the temperature profile shown in Figure 10a is representative throughout this period. Figure 10b shows the temporal variation of the cirrus cloud boundary altitudes derived from the 8.6-mm radar measurements between 2000 and 2400 UTC. A single layer of cirrus cloud was present during this time period. Between 2000 and 2100 UTC, the observed cloud top and base were located at 8 and 6 km, respectively. After 2100 UTC, the cloud top altitude fluctuates between 8 and 10 km, while the cloud base altitudes largely remains at 6 km, except for the period between 2130 and 2230 UTC. There are two clear/thin-cirrus episodes around 2100 and 2140-2200 UTC and one broken-cirrus period around 2210-2220 UTC. The retrieved cloud temperatures were converted into cloud altitudes using the temperature sounding shown in Figure 10a. For tracks 1 and 3, when WB-57F flew over the radar site, the area happened to be clear, although the radar recorded very thin cirrus. Thus, comparison of the retrieved cloud altitudes with the radar data cannot be accomplished. For tracks 5 and 8, the retrieved cloud temperatures over the radar site are $-33°$ and $-40°$C, which correspond to 8.2 and 9.2 km, respectively (denoted by square boxes in Figure 10b). Both altitudes are within the radar-derived cloud boundaries but near the cloud top at the particular WB-57F overpass time.

To verify the retrieved cirrus cloud optical depths and ice crystal mean effective sizes, we use the in situ ice crystal size distributions obtained by the optical probes on board the HARP to compute the single- scattering properties of the ice crystals and to evaluate the in situ mean effective size. A representative ice crystal size distribution has been constructed for each case by using the 2D-C probe measurements for ice crystals larger than 75 μm and an extrapolation technique for ice crystals smaller than 75 μm in a manner described in the following.

Among the cloud microphysical instruments on board HARP, the FSSP sizes the ice crystals from 1 to 96 μm; the 1D-C probe samples ice crystals from 20 to 300 μm; and the 2D-C probe measures the maximum dimensions of the projection of ice crystals from 25 to 800 μm. The size distributions derived from the 1D-C and 2D-C probes closely agree with each other for the size range of 25 to 300 μm, though the differences in the ice crystal number concentrations for some size bins can be as large as 1 order of magnitude. We choose to use the 2D-C derived ice crystal size distribution because this probe covers the typical ice crystal size range and because the FSSP derived size distributions appear to be unreliable in view of the unrealistically high ice crystal number concentrations for sizes less than 20 μm. For these reasons, we use the gamma function to extrapolate the 2D-C size distribution down to 1 μm to obtain the ice crystal size distribution for ice crystal sizes less than 75 μm [*Tsay et al.*, 1996]. Composite ice crystal size distributions combining the 2D-C probe measurements and the extrapolated portions are plotted in Figures 11a and 11b. The upper bound for both the ice crystal size distributions is less than 600 μm. Both ice crystal size distributions are similar to those occurring in typical cirrostratus clouds [*Heymsfield*, 1975]. We find that incorporating the extrapolated portion from 20 μm down to 1 μm has a negligible effect on the extinction coefficient. Other single-scattering parameters

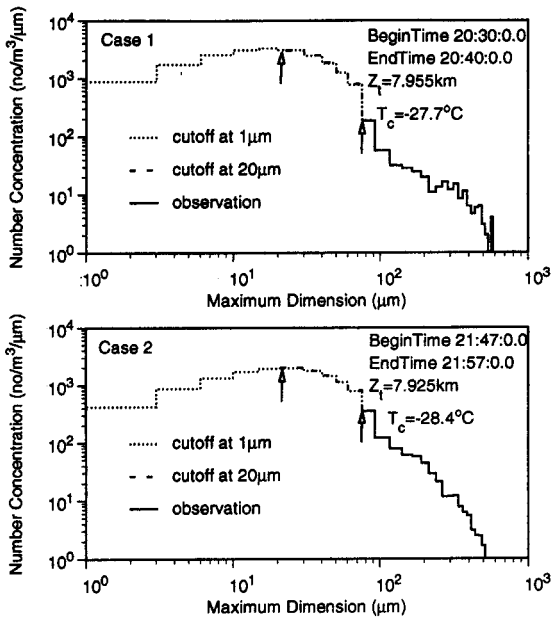

Figure 11. The ice crystal size distributions based on the HARP data (September 16, 1995) with the lower limit of 75 μm and extrapolations to 20 μm and 1 μm based on the gamma function and an optimization search method.

are not sensitive to the inclusion of ice crystals smaller than 75 μm for the size distributions used in the present study. Visible extinction coefficients of 0.54 and 0.57 km^{-1} were obtained for cases 1 and 2, respectively.

To determine the optical depth based on in situ measurements, the average cirrus cloud thickness and the associated extinction coefficients must be known. Based on the cloud boundary altitudes derived from the 8.6-mm radar measurements, the averaged cirrus cloud thicknesses during the two periods were about 1.75 and 2 km for cases 1 and 2, respectively. The ascending vertical profile of the 2D-C median volume ice crystal diameter indicates that ice crystal sizes vary by no more than 20 μm between 6.5 and 8 km [*Morrison et al.*, 1997]. For this reason, we use the computed extinction coefficients based on single-level in situ size distributions to represent the vertically averaged cirrus cloud extinction coefficients. The computed optical depths based on the preceding approximation are 0.94 and 1.14 for cases 1 and 2, respectively. The mean retrieved optical depths are 0.89 and 1.42 for tracks 1 and 3 of the ARES flight, respectively. The retrieved mean optical depth for track 1 agrees relatively well with that from the 2D-C probe. However, for track 3, the difference between the two optical depths is of the order of 0.3.

Finally, we utilize a cirrus cloud model composed of 50% bullet rosettes, 30% hollow columns, and 20% plates to compute the in situ mean effective ice crystal sizes. An empirical relationship between the maximum dimension (L) and width (W) is employed for each shape: for plates, $W = 2.02L^{0.449}$; for hollow columns, $W = 11.3L^{0.414}$ for $L > 200$ μm, $W = 8.479 + 1.002L - 0.00234L^2$ for $L < 200$ μm; and for bullet rosettes, $W = 2.3103L^{0.63}$. The in situ mean effective sizes are based on the average of the mean effective size for each shape weighted by the percentage distribution. They are 57.2 μm for case 1 and 55.2 μm for case 2. The retrieved mean effective sizes are 64.2 μm for track 1 and 53.3 μm for track 3, which compare reasonably well with the in situ sizes with differences less than 10 μm. There are two reasons for differences between retrieved and observation-derived optical depths and mean effective sizes. First, the estimate of the optical depth from the 2D-C probe is based on the composite ice crystal size distribution at a single flight level within the cirrus cloud. Second, the variation range of the retrieved optical depth for track 3 is much larger than that for track 1. To further validate the algorithm, more accurate measurements of collocated and coincident ice crystal size distributions, particularly in the small-particle range, are required.

4. Summary

We have presented a remote sensing algorithm for the retrieval of cirrus cloud temperature (height), optical depth, and ice crystal size using, for the first time, the spectral channels in the 5.1-5.3 μm range in combination with the 3.7 μm channel. This scheme has been applied to the ARES data collected on September 16, 1995, over the western Boston area. We have discussed the ARES channel spectral properties and the rationale for the selection of retrieval channels. Characteristics of the measured ARES channel data have been examined to demonstrate their suitability for retrieval. For retrieval purposes, a simple clear/cloud threshold detection scheme has been developed and applied to identify clear and cloudy data points.

Validation of the retrieved cirrus cloud height has been carried out by using the collocated and coincident time series of the cloud boundary (cloud top and base) altitudes derived from the ground-based 8.6 mm radar measurements. We have also compared the retrieved cirrus cloud optical depths and ice crystal mean effective sizes with those parameters determined based on the composite ice crystal size distributions from in situ measurements. We show that the retrieved cloud heights compare reasonably well with the values determined from the ground-based 8.6-mm radar, and that the retrieved optical depth and mean effective size match the values determined from the in situ microphysical measurements. Differences between the retrieved and observation-derived optical depths and mean effective sizes could be due to the limitation in data collection by aircraft and the inherent cloud horizontal and vertical inhomogeneity.

Acknowledgments. During the course of this work, our research programs have been supported by the Air Force Geophysical Directorate under contract F19628-96-C- 0052,

and in part by the AFOSR grant F49620-94-1-0142, and NASA grants NAG5-6160 and NAG5-6036.

References

Anderson, G. P., R. H. Picard, and J. H. Chetwind, Proceedings of the 17th Annual Review Conference on Atmospheric Transmission Models, *Spec. Rep.* 274, 332 pp. Phillips Lab/Geophy. Dir., Bedford, Mass., May 1995.

Baum, B. A., R. F. Arduini, B. A. Wielicki, P. Minnis, and S.-C. Tsay, Multilevel cloud retrieval using multispectral HIRS and AVHRR data: Nighttime oceanic analyses, *J. Geophys. Res., 99,* 5499-5514, 1994.

Fu, Q., and K. N. Liou, Parameterization of the radiative properties of cirrus clouds, *J. Atmos. Sci., 50,* 2008-2025, 1993.

Gao, B. C., and Y. J. Kaufman, Selection of a 1.375-μm channel for remote sensing of cirrus clouds and stratospheric aerosols from EOS/MODIS, *J. Atmos. Sci., 52,* 4231-4237, 1995.

Goody, R. M., and Y. L. Yung, *Atmospheric Radiation: Theoretical Basis,* 2nd ed., 519 pp., Oxford Univ. Press , New York, 1989.

Heymsfield, A., Cirrus uncinus generating cells and the evolution of cirriform clouds, I:, Aircraft observations of the growth of ice phase., *J. Atmos. Sci., 32,* 799-808, 1975.

King, M. D.,Y. J. Kaufman, W. P. Menzel, and D. Tanre, Remote sensing of cloud aerosol, and water vapor properties from the moderate resolution imaging spectrometer (MODIS), *IEEE Trans. Geosci. Remote Sens., 30,* 1-27, 1992.

King, M. D., et al., Airborne scanning spectrometer for remote sensing of cloud, aerosol, water vapor and surface properties, *J. Atmos. Oceanic Technol., 13,* 777-794, 1995.

Liou, K. N., *Radiative and Cloud Processes in the Atmosphere: Theory, Observation, and Modeling,* 487 pp., Oxford University Press, New York,1992.

Liou, K. N., S. C. Ou, Y. Takano, F. P. J. Valero, and T. P. Ackerman, Remote sounding of the tropical cirrus cloud temperature and optical depth using 6.5 and 10.5 μm radiometers during STEP, *J. Appl. Meteorol., 29,* 716-726, 1990.

Minnis, P., D. F. Young, K. Sassen, J. M. Alvarez, and C. J. Grund, The 27-28 October 1986 FIRE IFO cirrus case study: Cirrus parameter relationships derived from satellite and lidar data, *Mon. Weather Rev., 118,* 2402-2425, 1990.

Minnis, P., K. N. Liou, and Y Takano, Inference of cirrus cloud properties from satellite-observed visible and infrared radiances, *J. Atmos. Sci.,50,* 1279-1322, 1993.

Morrison, B. J., R. Hobbs, D. Rusk, J. Jung, and R. L. Rose, The High-Altitude Reconnaissance Platform (HARP), *SBIRS final report,* 264 pp., Aeromet, Inc., Tulsa, Okla. 1997.

Ou, S. C., K. N. Liou, W. M. Gooch, and Y. Takano, Remote sensing of cirrus cloud parameters using AVHRR 3.7- and 10.9-μm channels, *Appl. Opt., 32,* 2171-2180, 1993.

Ou, S. C., et al., Remote sounding of cirrus cloud optical depths and ice crystal sizes from AVHRR data: Verification using FIRE II IFO measurements, *J. Atmos. Sci., 52,* 4143-4158, 1995.

Rao, N. X., S. C. Ou, and K. N. Liou, Removal of the solar component in AVHRR 3.7-μm radiances for the retrieval of cirrus cloud parameters, *J. Appl. Meteorol., 34,* 482-499, 1995.

Takano, Y., and K. N. Liou, Radiative transfer in cirrus clouds, II. Theory and computation of multiple scattering in an anisotropic medium, *J. Atmos. Sci., 46,* 20-36, 1989.

Tsay, S.-C., P. M. Gabriel, M. D. King, and G. L. Stephens, Spectral reflectance and atmospheric energetics in cirrus-like clouds, II, Applications of a Fourier-Riccatti approach to radiative transfer, *J. Atmos. Sci.,53,* 3450-3467, 1996

Wielicki, B. A., P. Minnis, R. F. Arduini, L Parker, S.-C. Tsay, Y. Takano, and K. N. Liou, Remote sensing estimates of cirrus particle size for tropical and mid-latitude cirrus: Hexagonal crystals and ice spheres, paper presented at the FIRE Cirrus Science Conference, co-sponsored by NASA, NSF, NOAA, DOE, and ONR, Breckenridge, Colo., June 14-17, 1993.

Yang, P., and K. N. Liou, Finite-difference time domain method for light scattering by small ice crystals in three-dimensional space, *J. Opt. Soc. Am. A, 13,* 2072-2085, 1996a.

Yang, P., and K. N. Liou, Geometric-optics-integral-equation method for light scattering by nonspherical ice crystals, *Appl. Opt., 35,* 6568- 6584, 1996b.

K. N., Liou, S. C. Ou, P. Rolland, and P. Yang, Department of Atmospheric Sciences, 7127 Math Science Building, 405 Hilgard Avenue, University of California at Los Angeles, Los Angeles, CA 90095-1565, (e-mail: knliou@atmos.ucla.edu; ssou@atmos.ucla.edu; prolland@atmos.ucla.edu; yang@micro.atmos.ucla.edu)

T. R. Caudill, Air Force Research Laboratory/VSBE, 29 Randolph Road, Hanscom Air Force Base, MA 01731-3010 (e-mmail : caudill@plh.af.mil)

J. Lisowsky, SciTec, Inc., 100 Wall Street, Princeton, NJ 08540 (e-mail : jjl@scitec.com)

B. J. Morrison, Aeromet, Inc., P. O. Box 701767, Tulsa, OK 74170-1767 (e-mail : brianm@aeromet.com)

(Received January 6, 1998; revised May 29, 1998; accepted June 4, 1998.)